Materials Science & Engineering C 111 (2020) 110842

Contents lists available at ScienceDirect

Materials Science & Engineering C

journal homepage: www.elsevier.com/locate/msec

Injectable supramolecular nanohydrogel from a micellar self-assembling calix[4]arene derivative and curcumin for a sustained drug release

Giuseppe Granata[a], Salvatore Petralia[b,*], Giuseppe Forte[c], Sabrina Conoci[d], Grazia Maria Letizia Consoli[a,*]

[a] Institute of Biomolecular Chemistry-C.N.R., Via P. Gaifami 18, 95126 Catania, Italy
[b] STMicroelectronics, Stradale Primosole 50, 95121 Catania, Italy
[c] Department of Drug Science, University of Catania, Viale Andrea Doria 6, 95125 Catania, Italy
[d] Department of Chemical, Biological, Pharmaceutical and Environmental Science, University of Messina, 98166 Messina, Italy

ARTICLE INFO

Keywords:
Injectable nanohydrogel
Self-assembling calix[4]arene
Micelle
Curcumin
Drug delivery

ABSTRACT

In the search for soft and smart materials for nanomedicine, which is a present challenge, supramolecular nanohydrogels built on self-assembling low-molecular-weight building blocks attract interest for their structural, mechanical and functional properties. Herein, we describe a supramolecular nanohydrogel formed by a biofriendly micellar self-assembling choline-calix[4]arene derivative in the presence of curcumin, a natural and multitarget pharmacologically relevant drug. Morphology and mechanical properties of the nanohydrogel were investigated, and theoretical simulation performed to model the nanohydrogel structure. The self-healing and injectable nanohydrogel easily formed in PBS medium at physiologic pH, without using additives and organic solvents. The micellar nanohydrogel protected curcumin from rapid chemical and photochemical degradation, and slowly dissolved in curcumin-loaded micelles sustaining the drug release in a low rate. The nanohydrogel which combines the mechanical properties of a hydrogel and the benefits of a nanoscale micelle in drug delivery, appears a promising novel material for drug delivery.

1. Introduction

In the field of materials science for medicine, hydrogels have turned out smart materials for a variety of applications and have found enormous clinical use [1–3]. Hydrogels are highly hydrated materials produced through chemical and/or physical crosslinking of molecules forming three-dimensional networks entrapping the solvent. They by combining the elastic behaviour of solids with the microviscous properties of fluids, can create a reservoir of drug and facilitate the local and sustained drug delivery, that can result in an improved therapeutic efficacy and reduction of the undesired effects of a systemic drug administration.

Supramolecular hydrogels, formed through reversible, non-covalent intermolecular interactions, are very attractive for biomedical applications [4,5]. Loh labeled supramolecular hydrogels as “part of the next-generation of materials to enter the biomedical arena” [6]. Supramolecular hydrogels do not require laborious syntheses and exhibit properties different from their covalent counterpart such as facile formation, hierarchical organization, and stimuli responsiveness that have shown to considerably enhance the therapeutic outcome of drug delivery [7].

Supramolecular nanohydrogels formed by a gel matrix containing the drug loaded into nanoparticles [8], represent an advancement as drug delivery devices, because they combine the mechanical properties of a hydrogel with the advantages of a nanoparticle that as a nanocontainer and a nanocarrier can improve drug delivery [9]. Generally, nanohydrogels are formed by drug-loaded nanoparticles mixed to a gel matrix [10], but there is a growing interest in nanohydrogels generated by molecules self-assembling in nanoparticles able to entrap a drug and form a gel without addition of additives [11].

Calix[*n*]arenes are polyphenolic macrocycles of interest in supramolecular chemistry [12]. The opportune functionalization of the calixarene skeleton has provided derivatives with a wide spectrum of applications in different areas [13]. In biomedical and pharmaceutical fields [14,15], calix[*n*]arene derivatives have shown promising therapeutic [16], imaging [17], and drug delivery functions [18]. Analogously to cyclodextrins and cucurbituril, calix[*n*]arene macrocycles are interesting low-molecular-weight building blocks for the construction of supramolecular gels equipped with additional receptor sites and stimuli responsiveness, in which self-assembling and inclusion

* Corresponding authors.
E-mail addresses: salvatore.petralia@st.com (S. Petralia), grazia.consoli@icb.cnr.it (G.M.L. Consoli).

https://doi.org/10.1016/j.msec.2020.110842
Received 8 October 2019; Received in revised form 27 February 2020; Accepted 11 March 2020
Available online 12 March 2020
0928-4931/

complexes exploiting the host properties of the macrocycle cavity drive the hydrogel formation [19]. Several works reported calix[*n*]arene derivatives forming hydrogels [20–22], but to the best of our knowledge only two papers described supramolecular hydrogels formed from calixarene-based micelles. They concern a micellar proline-functionalised calix[4]arene, whose gelation was controlled by non-covalent interactions with amino acids in acidic condition [23]; and a sulfonate calix[4]arene grafted to polymer chains with gelation driven by the strong binding between calixarene cavities and viologen moieties on the polymer [24].

Here, we report a novel supramolecular nanohydrogel derived from spontaneous gelation of a micellar polycationic choline-calix[4]arene derivative **1** (Calix) [25] in the presence of curcumin (Cur) in phosphate buffered saline (PBS) at pH 7.4, under stimulus concentration.

Curcumin is a natural polyphenolic multitarget drug with a multiplicity of pharmacological applications, but poor aqueous solubility, rapid degradation and low bioavailability constitute major obstacles toward its deployment in medicine [26]. For this reason, the search for novel formulations designed for overcoming these limitations and improving the pharmacological performance of curcumin is still a challenge. Since a highly concentrated application of polyphenols may result in a toxic response, another problematic of curcumin is the mode of application. A formulation with controlled release property, as a hydrogel can be, is preferred for the clinical application of this drug. In this context, the Calix-Cur nanohydrogel appears a promising candidate. It is formed by biofriendly components: a choline-calix[4]arene derivative (**1**) whose no significant cytotoxicity was previously proved [27–29]; curcumin, a natural drug; and a biomimetic medium like PBS at physiological pH value. Interestingly, the presence of choline ligands on the surface of the calixarene micelle makes the nanohydrogel also a promising new tool for targeted drug delivery. Indeed, it is known that the choline ligand can favour the crossing of cellular membranes and anatomical barriers and can target cells on which choline transporters are over-expressed [30].

In this work we describe the preparation of the Calix-Cur supramolecular nanohydrogel and investigate its morphology and structure by Atomic Force Microscopy (AFM) and Transmission Electron Microscopy (TEM), UV–vis and fluorescence spectroscopy and molecular modelling simulations supported by TD-DFT UV–vis spectra. The capability of the nanohydrogel to preserve curcumin from rapid degradation and slow down the drug photodegradation is evaluated by chromatographic (HPLC) monitoring and steady-state photolysis, respectively. The mechanical properties of the nanohydrogel are investigated by rheological measurements. The hydrogel dissolution related to drug release is explored by chromatographic (HPLC) and Dynamic Light Scattering (DLS) analyses.

2. Experimental section

2.1. Materials

Curcumin (Cur) and all the other chemicals were purchased from Sigma-Aldrich (Milan, Italy) and used without purification. Solvents were of analytical or high-performance liquid chromatography (HPLC) grade. Choline-calix[4]arene derivative **1** (Calix) was prepared as reported in literature [25].

2.2. Preparation of Calix-Cur hydrogel

For the preparation of Calix-Cur hydrogel, 100 mg of choline-calix[4]arene derivative **1** was dissolved in 5 mL PBS (10 mM, pH 7.4) and curcumin (9.1 mg) was added. The mixture was sonicated for 15 min, then stirred (500 rpm) at 37 °C up to complete dissolution of the Cur.

2.3. Stability and photostability of Cur in the hydrogel

To evaluate the stability of Cur in the hydrogel, the amount of Cur was monitored by HPLC analysis over time by using a Dionex HPLC system (P680 pump, ASI-100 autosampler, UVD170U detector, TCC-100 temperature-controlled column compartment), and Phenomenex Luna 5 μm C18 reverse-phase column (250 × 4.6 mm). Eluents A: CH_3CN, B: 0.25% AcOH, gradient: A from 40% to 76%, 18 min, flow 1 mL/min, T = 48 °C, λ = 425 nm. 32.7 mg of Calix-Cur hydrogel were dissolved in 1 mL of ethanol, then 50 μL of this solution were diluted with 550 μL di CH_3CN, and 40 μL of sample were injected. To evaluate the photostability of Cur loaded into the nanohydrogel, steady-state photolysis analyses (λ_{exc} = 420 nm) were performed. An aliquot of Calix-Cur hydrogel sample was deposed on cleaned quartz substrate, to form a uniform film, and the changes in the absorption spectra upon exposure at 420 nm were evaluated. For comparison the changes in the absorption spectral of freshly prepared Cur solution in 10% ethanol/PBS were also evaluated.

2.4. Atomic Force Microscopy (AFM)

AFM analysis was performed with PSIAXE-150, acquiring images of 1 μm × 1 μm. The measurements were carried out in non-contact mode using a silicon, Sn doped tip. It has a resistivity of 0.01 Ω cm and was purchased by Bruker TESPAW. The tip dimensions are: thickness 4 μm, length 125 μm, width 40 μm. The stiffness is 40 N/m and it was operated to an oscillation frequency of 320 kHz.

2.5. Transmission Electron Microscopy (TEM)

The morphology of the Calix − Cur hydrogel was analysed under a ATEMJEOL JEM-2010 instrument equipped with a therm ionic source of lanthanum hexaboride and using bright field in conventional parallel beam mode. The samples were prepared dispensing large and low amount of hydrogel on grid surface.

2.6. Hydrogel UV–Vis and fluorescence measurements

UV–Vis spectra absorption and fluorescence emission spectra were recorded with a JascoV-560 spectrophotometer and a Spex Fluorolog-2 (mod. F-111) spectrofluorometer, respectively, in air equilibrated solutions, using either quartz cells with a path length of 1 cm and quartz substrates.

2.7. QM simulations

In the simulation study the molecule of Cur was considered in the monoanion-enol form (Cur^{-1}). Since Cur^{-1} is planar and shows a conjugated double bond system, we have considered four different orientations of the Cur with respect to the Calix. The Calix-Cur nanoassemblies were fully optimized at the CAM-B3LYP/6-31G(d) level [31,32] and the Polarizable Continuum Model (PCM) [33,34] was used to calculate the solvent effect. When molecules interact, the non-covalent attraction contains dispersion forces, arising from instantaneous charge fluctuations, dipole-induced dipole forces and dipole-dipole forces (including hydrogen bonding). CAM-B3LYP is a hybrid exchange-correlation functional which well predicts the strength of non-covalent interactions [35-37]. UV–vis spectra were performed, on the optimized structures, within the time-dependent DFT approach (TD-DFT) [38,39] adopting the 6-31G(d)basis set and the B3LYP functional which has been used successfully to simulate UV-VIS spectra of Cur and Cur derivatives [40-43]. Gibbs free energies in solution were calculated at the CAM-B3LYP/6-31G(d) level using the SMD method developed by Truhlar et al. [44].

2.8. Rheological measurements

Rheological experiments were carried out on a CVO rheometer (Bohlin Instruments, Malvern, UK) with 4°/40 mm diameter steel cone-plate geometry, at 25 °C (where not clearly expressed), and the results were analysed by Bohlin R6.51.03 software. The storage (G′) and loss (G″) moduli were monitored by frequency sweep at 2% strain with varying angular frequency (1–25 rad/s). Amplitude sweep from 1 to 100% strain at constant 10 rad/s was also performed on the sample.

The viscosity variation was conducted from 0.1 to 100 s^{-1} shear rate. The consistency index (K) and the flow behaviour index (n) were evaluated by fitting ($R^2 = 0.999$) the rheological data (from 2.2 to 100 s^{-1} shear rate, shear-thinning linear part of log-log plot) by the power law model:

$$\eta = K \cdot \dot{\gamma}^{n-1}$$

where η is the apparent viscosity and γ is the shear rate.

For self-healing experiments, amplitude sweep from 1 to 3000% strain at a frequency of 1 s^{-1} was performed on the samples to gel failure, then recovery was monitored at 1% strain (1 s^{-1} frequency) for 740 s. To mimic shear forces that would be exerted on a sample during a syringe injection, the shear rate was rapidly increased (from 1 to 1000 s^{-1} in 10 s), then a steady shear (1000 s^{-1} for 30 s) was applied to the hydrogel. After the shear rate was decreased to 1 s^{-1} in 10 s, and stopped for 50 s. Finally, the recovery was monitored at 1 s^{-1} for 30 min.

2.9. Hydrogel dissolving (%)

The gel dissolving (%) was calculated by Cur quantification in the release medium. To monitor the release of Cur at different time (from 6 to 72 h), 7 vials (1.5 mL) were filled with 170 mg of hydrogel and 340 μL of 10 mM PBS were added to each vial. The samples were placed in a shaker at 37 °C and stirred at 100 rpm. The stirring was stopped and 50 or 20 μL of each supernatant were withdrawn and diluted with 50 μL of acetonitrile. Cur was quantified by using the before described HPLC conditions (injection volume 50 μL). Since the dissolution of the hydrogel mainly occurs at the interface between the hydrogel surface and the release medium, we assumed that the value of hydrogel dissolving percentage is dependent on the hydrogel thickness, and corresponds to the released Cur (%) calculated by the following formula:

$$Cur\ release\ (\%) = \frac{\text{Amount of Cur in the release medium}}{\text{Amount of total Cur}} \times 100$$

The gel dissolving (%) showed linear behaviour in function of time (t) ($R^2 = 0.992$):

$$Gel\ dissolving\ (\%) = \frac{k}{a} \times t$$

where k indicates the amount (%) of gel dissolved/h relative to a gel sample of 1 mm thickness; a indicates the gel thickness in mm.

2.10. Dynamic light scattering (DLS) and electrophoretic light scattering (ELS)

The presence of nanoaggregates in the release medium and the measurement of their size, polydispersity index and zeta potential were investigated by DLS and ELS by using a ZetaSizer NanoZS90 Malvern Instrument (UK), equipped with a 633 nm laser, at the scattering angle of 90° and 25 °C temperature. Each measurement was performed three times.

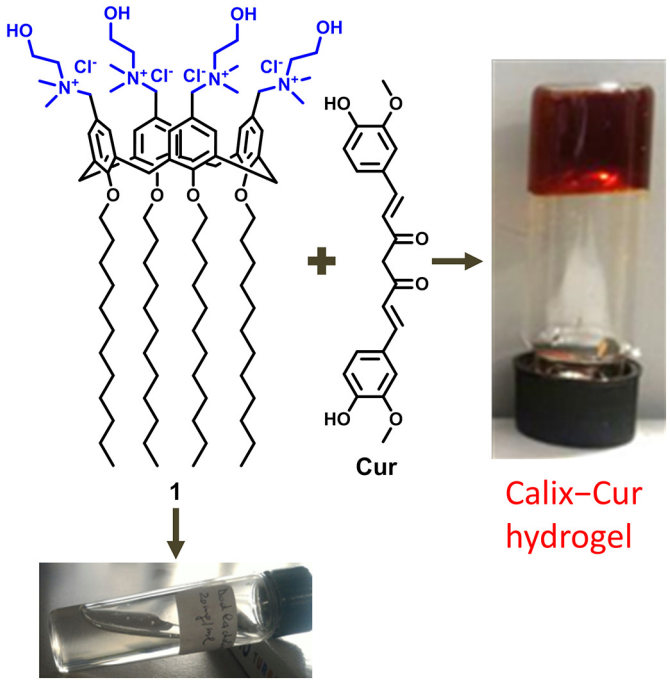

Fig. 1. Molecular representation of Calix **1** and curcumin, and photograph of Calix **1** colloidal solution and Calix-Cur hydrogel.

3. Results and discussion

3.1. Hydrogel formation

Calix[4]arene derivatives bearing choline moieties at the upper rim and alkyl chains at the lower rim, are a class of amphiphilic calixarenes self-assembling in globular micelles whose potential as gene [29] and drug vehicles [45,46] has been demonstrated. In a previous paper, we reported that amphiphilic choline-calix[4]arene derivative **1** (Calix), by simple dissolution in PBS medium, forms micellar nanoaggregates [25] capable to load curcumin (Cur) and significantly improve the drug water solubility (about 0.1 mg/mL of Cur per mg/mL of Calix) and chemical stability [27].

Interestingly, we observed that increasing the concentration of Calix **1** (20 mg/mL) and Cur (1.8 mg/mL) in 10 mM PBS (pH 7.4), a clear reddish hydrogel, not flowing down in the inverted vial (Fig. 1), rather than a colloidal solution, formed.

In the hydrogel the maximum amount of solubilized Cur corresponds to a drug loading percentage around 9%. Since Calix **1** alone does not form hydrogel also at concentrations higher than 20 mg/mL, it was evident that Cur acts as a gelator. Noteworthy, the stable and transparent Calix-Cur hydrogel forms by simple dissolution of Cur in the micellar colloidal solution of Calix **1** without using particular techniques, additives or organic solvents generally used to solubilize curcumin.

3.2. Calix-Cur hydrogel structure

Hydrogels structured at nanometer level are a topic of interest in materials science, since they exhibit interesting properties not only from the mechanical but also from the functional point of view [47].

Since the Calix **1** alone [25] and in the presence of Cur [27] in PBS medium generates a colloidal solution containing micellar nanoaggregates, a micelle-based structure for the Calix-Cur hydrogel could be easily hypothesized. The presence of micellar nanodomains in the Calix-Cur hydrogel was immediately evidenced by microscopic images.

TEM images showed macroscopic structures typical for hydrogels in a sample prepared with large amount of Calix-Cur hydrogel (Fig. 2a, the

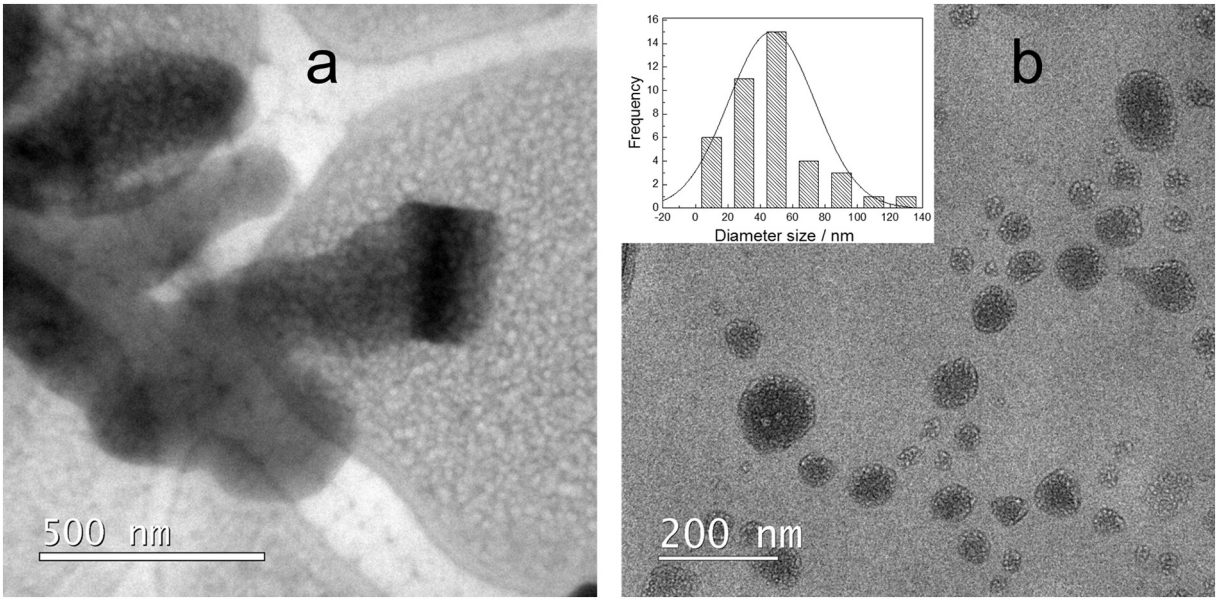

Fig. 2. TEM images of the Calix-Cur hydrogel: at large- (a) and low-amount (b).

dark structures were assigned to the salt residues), and spherical aggregates (Fig. 2b) with a size distribution centred at 44 nm (Fig. 2b inset) in a sample prepared with a lower amount of hydrogel. The size distribution analysis evidenced the presence of small aggregates with diameter of 6–7 nm, ascribable to single micelles, and larger structures with diameter higher than 80 nm, assignable to aggregates of micelles. The presence of spherical nanoaggregates in the hydrogel was also evident in AFM images (see SI, fig. S1).

To gain insight on the location of Cur in the reddish micellar nanohydrogel, we performed molecular modelling simulations supported by TD-DFT UV–vis spectra. Since it is known that the β-diketone form of Cur is featured by a yellowish colour while the anionic enol form has a reddish-orange colour [48,49], this latter form (Cur^{-1}) was taken in consideration for *ab initio* calculations. The globular structure of the nanoaggregates suggested four main hosting sites for Cur: the interfacial region, the calix[4]arene cavity, the palisade layer and the inner core.

Theoretical simulations provided four models depicted in Fig. 3: two *bridge models* where the phenolic oxygens of Cur face the quaternary ammonium cations decorating the cavity of two Calix units belonging to two different micelles (B1 and B2 in Figs. 3a and b), and two *sandiwich models* (S1 and S2 in Fig. 3c and d) where one Cur^{-1} molecule is sandwiched between two Calix units in the same micelle.

The absorption spectrum (Fig. 4A) simulated for anionic Cur^{-1} (412 nm), S1 (425 nm), S2 (467 nm), B1 (481 nm) and B2 (482 nm) models accorded the optical absorption spectrum recorded for the Calix-Cur hydrogel (Fig. 4B-a), which shows absence of absorption at 366 nm, reasonably excluding the presence of the β-diketone structures, two main absorption peaks centred at 425 and 467 nm, and broad bands at around 482 nm. The optical absorption and fluorescence emission spectrum of Calix-Cur hydrogel are reported in Fig. 4B-a and 4B-b respectively.

Data summarized in Table 1 indicate a slight red shift of the curcumin absorption band for the S1 model (425 nm), which is characterized by weak interactions between Cur and Calix, and a stronger red shift for the S2 model (467 nm) where both H-bond (involving the Calix-CH_2-OH and the methoxy oxygen of Cur) and ion-dipole interactions (between the quaternary ammonium cation of Calix and phenolic hydroxyl oxygen of Cur) are present. In the case of the bridged model B1, both O-H-bonds and aromatic hydrogen bonds between Calix and Cur shift the absorption band to 481 nm, while for the B2 model H-bond and ion-dipole interactions shift the absorption band to 482 nm. A similar red shift was observed for anionic Cur entrapped in cationic micelles [50] or β-amiloid aggregates [48,51].

For the weak Calix-Cur interactions, which do not affect significantly the UV–vis spectrum, we observed an absorption concerning the H➔L electronic transition (S1); differently for the stronger interactions the absorption involves the electronic transition between H-1 and L energy levels (S2, B1 and B2 in Table 1).

The values of the atomic charges of phenoxy and methoxy oxygens and β-carbon-enol atom of Cur (Table 2), calculated by using the Merz–Singh–Kollman scheme [52,53], were also indicative of an appreciable interaction of Cur with Calix **1**. A noticeable atomic charge variation was observed for the bridge structures B1 and B2 with a marked decreasing of charge for the β-carbon-enol atom (average value 0.134 e), a medium increasing of charges for the phenoxy oxygen (average values 0.060 e and 0.071 e, ring 1 and 2) and a slightly increasing of charges for the methoxy oxygen atoms (average values 0.037 e and 0.024 e, ring 1 and 2). The sandwiched structures (S1 and S2) report a less marked atomic charge variations. The free energy for the formation of the Calix-Cur models in water solvent, clearly indicate an effectiveness binding for Calix-Cur on the bridge models (ΔG° values of $-3{,}7\ kcal\ mol^{-1}$ and $-2.9\ kcal\ mol^{-1}$ for B1 and B2, respectively) respect to the sandwiched models (ΔG° values of $-1.9\ kcal\ mol^{-1}$ and $-1.8\ kcal\ mol^{-1}$ for S1 and S2, respectively).

The entrapment of Cur in the hydrogel matrix was also corroborated by the fluorescence emission spectrum of the Calix-Cur hydrogel (λ_{exc} = 412 nm, λ_{em} = 625 nm), showing the red-shift of Cur emission maximum from 540 nm, typical of free Cur, to 625 nm (Fig. 4B-b). A similar shift (610 nm) was also observed for Cur in the Calix−Cur micellar colloidal solution [27].

Therefore, about the hydrogel formation, it is plausible that at higher concentrations of Calix and Cur, a molecule of anionic curcumin with its symmetric structure interacts with the cationic groups decorating the cavities of two Calix units belonging to different micelles, leading to the formation of secondary assemblies. The join of these assemblies, also favored by inter-micellar hydrogen bonds involving the choline hydroxl groups, generates a three-dimensional network that by retaining water through surface tension effect, leads to the formation of a supramolecular micellar nanohydrogel (Fig. 3e).

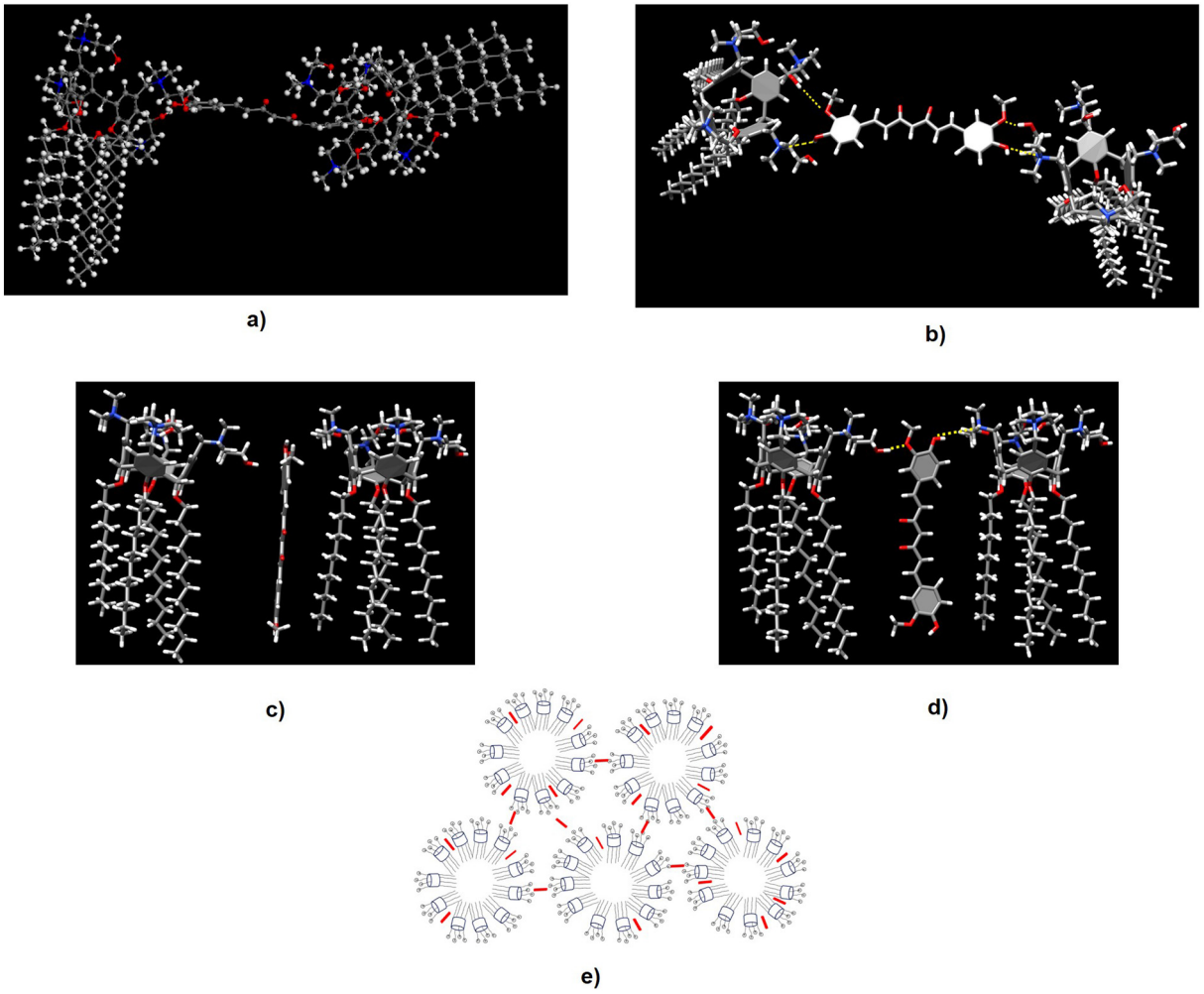

Fig. 3. Simulation Modelling for Calix-Cur interactions in PBS medium: bridge B1 model (a), bridge B2 model (b), sandwich S1 model (c) and sandwich S2 model (d). Schematic illustration of the hypothesized structure of the micellar Calix-Cur nanohydrogel (e). The red bars symbolize curcumin in sandwiches and bridge models. (For interpretation of the references to colour in this figure legend, the reader is referred to the web version of this article.)

3.3. Curcumin stabilization

The physico-chemical instability of Cur is a factor limiting its use. The entrapment in nanostructured systems is a potential approach for preserving Cur from acidic/alkaline degradation, oxidation and photodegradation.

In a previously study, we demonstrated that the entrapment of Cur in the micelle of Calix **1**, significantly reduces Cur degradation [27] reported to be approximately 90% within 30 min in PBS at 37 °C [54]. A similar behaviour was observed for the hydrogel that stored in the dark at room temperature preserved Cur for weeks.

Since the development of formulations for the photoprotection of

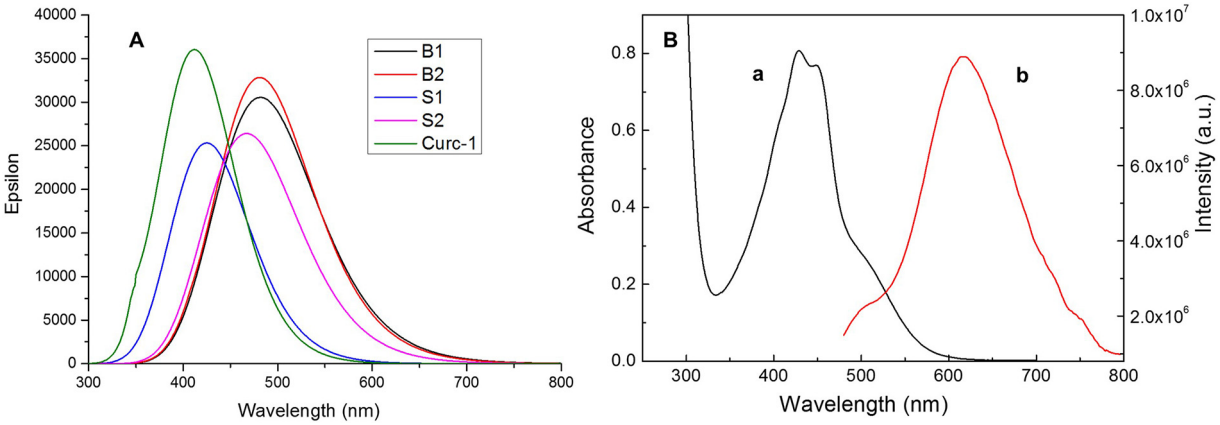

Fig. 4. (A) UV–Vis simulated absorption spectrum for Cur^{-1} (412 nm), S1 (425 nm), S2 (467 nm), B1 (481 nm) and B2 (482 nm) models. (B) Calix-Cur hydrogel: a) UV–vis absorption spectrum and b) emission spectrum (λ_{exc} = 412 nm; λ_{em} = 625 nm).

Table 1
Absorption (λ), oscillatory strength (f) and Homo-Lumo transition of Cur and Calix-Cur simulated models (see ESI, Fig. S2).

Compound	λ calc. (nm)	f calc.	Transition
Cur^{-1}	412	1.153	H➔ L
S1	425	0.615	H ➔ L
S2	467	0.651	H-1➔ L
B1	481	0.739	H-1– > L
B2	482	0.755	H-1 ➔ L

Table. 2
Main atomic charges (a. u.) of Cur and Calix-Cur simulated models.

Structures	Me-O (ring1)	Ar-O (ring1)	Enol group	Me-O (ring2)	Ar-O (ring2)
Cur^{-1}	−0.256	−0.535	−0.848	−0.256	−0.535
S1	−0.266	−0.556	−0.737	−0.274	−0.575
S2	−0.268	−0.547	−0.796	−0.281	−0.569
B1	−0.287	−0.597	−0.719	−0.279	−0.609
B2	−0.293	−0.593	−0.710	−0.280	−0.603

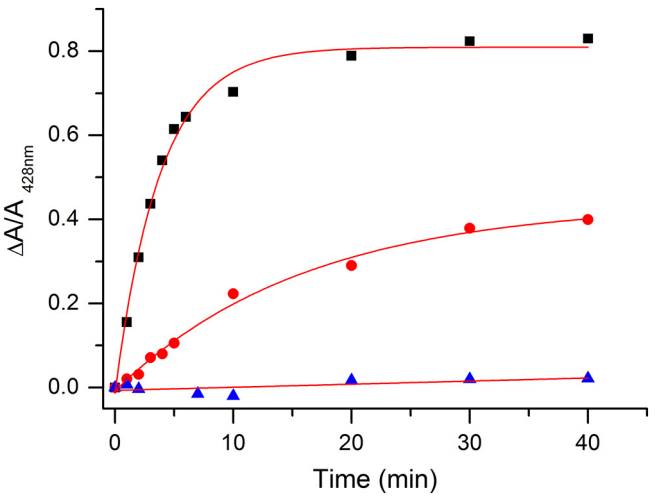

Fig. 5. Normalized absorbance decrease observed upon exposure of a 10% ethanol-PBS solution of Cur (black squares) and Calix-Cur hydrogel (red circle) at λ_{exc} = 420 nm for regular intervals of 40 min. A light-blank sample of the Calix-Cur hydrogel in darkness (blue triangles). (For interpretation of the references to colour in this figure legend, the reader is referred to the web version of this article.)

Cur is a challenge, we evaluated the capability of the hydrogel to protect Cur from its high sensitivity to light. The Cur photoprotection was investigated by steady-state photolysis. The experimental data in Fig. 5 show a very fast photodegradation for free Cur (Fig. 5 black squares) and a photodegradation of 40% after 40 min of exposure for Cur in the hydrogel (Fig. 5 red circles). The absorption spectral changes upon exposure of the Cur-loaded hydrogel to visible light (λ_{exc} = 420 nm) for regular intervals of 40 min are showed in ESI (Fig. S3) compared with an aqueous alcoholic solution of Cur (Fig. S4).

3.4. Hydrogel mechanical characterization

Rheological analyses were performed to achieve information on the mechanical properties of the Calix-Cur hydrogel. The viscoelastic behaviour was analysed by oscillatory rheological measurements.

The storage modulus (G′) values larger than the loss modulus (G″) values, and no significant changes of G′ and G″ values within the applied range of angular frequency, were indicative of a viscoelastic and stable hydrogel (Fig. 6a). The elastic nature of the hydrogel was also corroborated by G′ and G″ values never intersecting each other throughout 1–100% strain range and constant rad/s angular frequency (Fig. 6b).

The hydrogel exhibited the typical rheological behaviour of a non-Newtonian pseudoplastic fluid, indeed its apparent viscosity decreased rapidly with the increase of the shear rate (Fig. 7). The consistency index (K) was calculated to be 7.2 ± 0.1 Pa·s^n (n = 0.13 ± 0.01) by using the Ostwald – de Waele or power law [55].

Thixotropic hydrogels flow when introduced to a steep change in shear rate, to return to a gel state after a finite time under static conditions. The thixotropic behaviour of the Calix-Cur hydrogel at 25 °C and 37 °C, was evidenced by forward and backward rheograms showed in ESI (Fig. S5).

The supramolecular Calix-Cur hydrogel possesses self-healing property that refers to the partial or complete reforming of broken bonds in a spontaneous manner to restore the original structure. Upon the application of a large amplitude oscillatory strain, both G′ and G″ values decreased and G′ became lower than G″, indicating a network destruction. The failure of the hydrogel was observed at about 1500% strain. When the applied strain was returned to 1%, the recovery of both G′ and G″ within seconds was indicative of a rapid self-healing (Fig. 8). The self-healing behaviour of the Calix-Cur hydrogel was corroborated by alternate step strain sweep test, performed at a frequency of 1 s^{-1} and amplitude oscillatory strains from 1% to 1800% (see ESI fig. S6) [56–58].

The self-healing is typical of injectable hydrogels that are appealing for pharmaceutical applications as they can self-adapting in the space inside the injection site [59]. To confirm the hydrogel injectability, a steady shear was applied to the Calix-Cur hydrogel to mimic shear forces that would be exerted on a sample during a syringe injection. Fig. 9 shows the decrease of viscosity under shear (1000 s^{-1} for 30 s) and the recovery of the mechanical properties, monitored at 1 s^{-1} for 30 min, once coming to rest.

The viscoelastic behaviour and the failure and recovery properties of the hydrogel were corroborated by a creep-recovery, showing that when the stress was relieved (t_1 = 300 s), the strain immediately decreased and continued decreasing gradually to a residual strain (see ESI, Fig. S7).

The balance of adhesion (substrate-surface interaction) and cohesion (intermolecular interactions) plays a significant role in the adhesiveness of a hydrogel destined to topical application [60]. Such a balance should be maintained to a prolonged retention time at the site of administration. The cohesive and adhesive properties of the Calix-Cur hydrogel were suggested by qualitative analyses. Fig. 10 shows the cohesive property of the hydrogel by adhesive separation characterized by the formation of a fibrillar structure [61], and the hydrogel adhesiveness and capability to accommodate skin surface roughness.

3.5. Hydrogel dissolution

The Calix-Cur hydrogel was stable to heating as corroborated by negligible changes of the optical absorption at 75 °C (see ESI, Fig. S8). A high viscous solution was obtained only increasing the temperature over 75 °C. This conversion was reversible, and the hydrogel reformed upon cooling to 25 °C (see ESI, Fig. S9).

To investigate the dissolution of the Calix-Cur hydrogel, PBS was added to a known amount of hydrogel placed into a vial. The dissolution rate was measured by dosing the amount of Cur in the supernatant by HPLC analyses. Fig. 11 shows that Cur is slowly released (0.30 ± 0.02%/h × mm of hydrogel thickness) from the hydrogel incubated at 37 °C.

Considering the micellar structure of the nanohydrogel and the previously demonstrated ability of the Calix **1** micelle to load and preserve Cur from rapid degradation in PBS [27], it is plausible that the dissolution of the hydrogel occurs through the release of micellar nanoaggregates containing Cur. This was corroborated by dynamic light

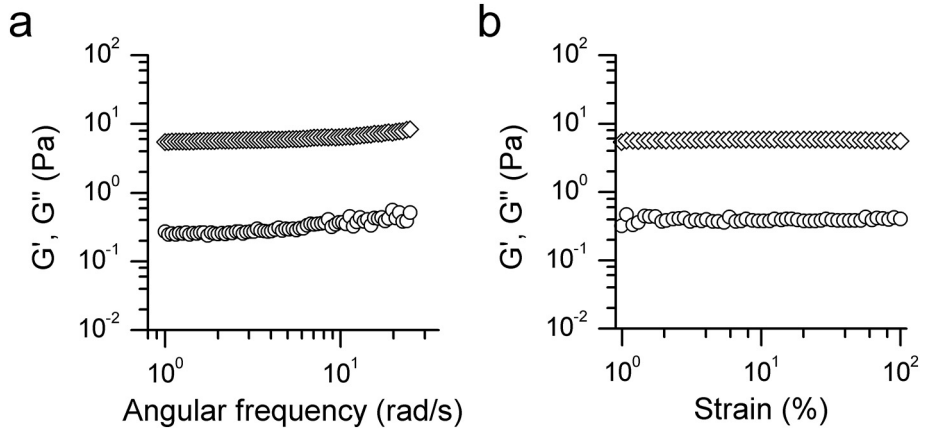

Fig. 6. Rheological analysis of the Calix-Cur hydrogel at 25 °C. Storage (diamond) and loss (circle) moduli acquired at constant 2% strain and increasing angular frequency (a); and at constant frequency and increasing strain % (b).

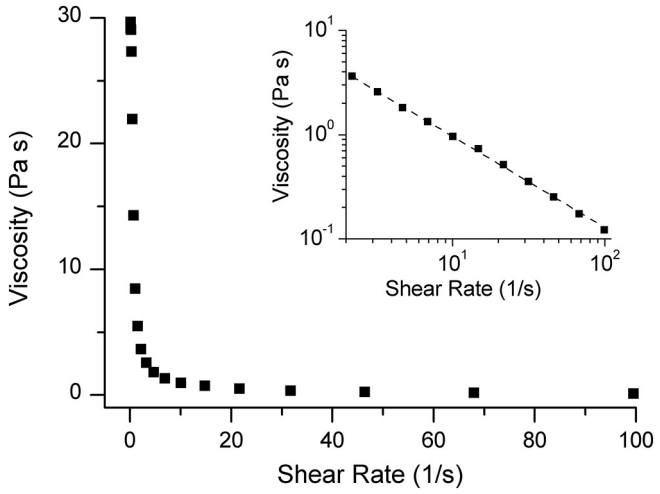

Fig. 7. Viscosity variation of the Calix-Cur hydrogel as a function of shear rate. Insert shows the plot obtained by fitting the viscosity variation by power-law model (logarithm scale).

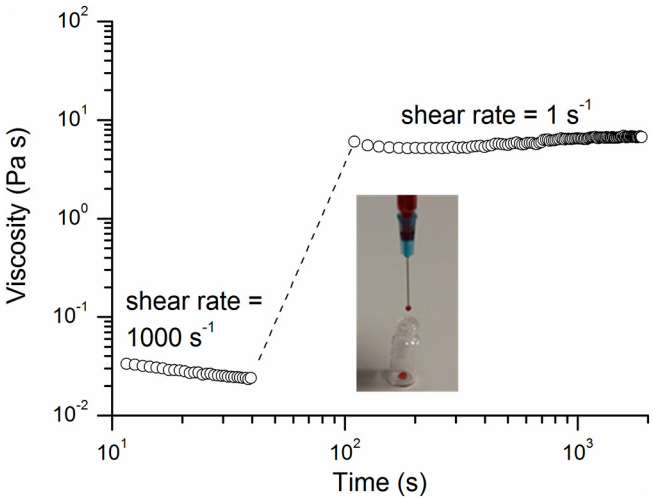

Fig. 9. Rheological analysis showing the self-healing of the Calix-Cur hydrogel after 1000 s^{-1} steady shear rate, at 25 °C; and photograph of the hydrogel flowing through a needle attached to a syringe.

scattering and electrophoretic mobility measurements showing the presence of nanoaggregates with mean hydrodynamic diameter around 90 nm (Z average) (Fig. 11 inset) and zeta potential of +23 mV in the release medium. These values and the stability of Cur over time were very similar to those found for the previously reported micellar Calix **1**-Cur colloidal solution [27]. The dissolution of the nanohydrogel in curcumin-loaded micellar nanoaggregates whose anti-inflammatory activity we previously proved *in vitro* and *in vivo*, applied as eye drop in the eyes of rats with LPS-induced uveitis [27], strongly supports the potential of the nanohydrogel in pharmaceutical field.

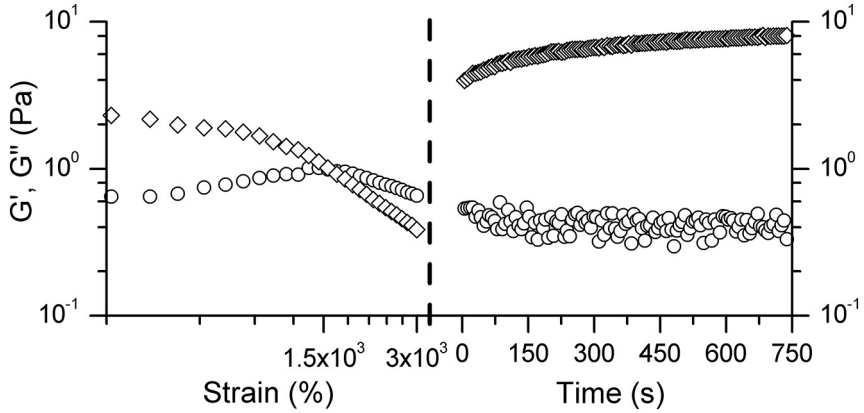

Fig. 8. Self-healing properties of the Calix-Cur hydrogel at 25 °C. Strain is reported from 310% to 3000% at frequency 1 s^{-1} and the recovery was monitored at 1% strain at frequency 1 s^{-1} (G′ diamond, G″ circle).

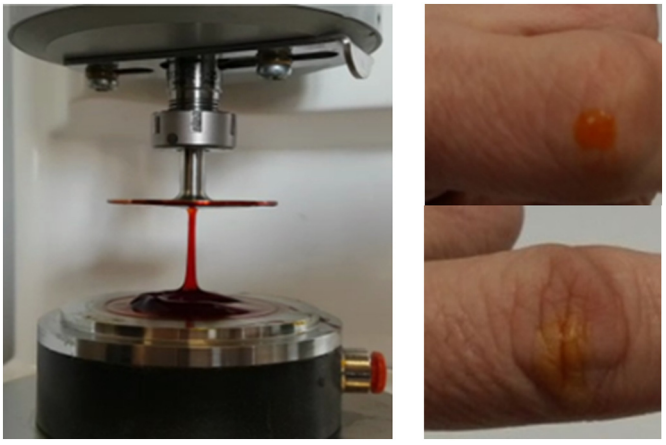

Fig. 10. Photographs of the Calix-Cur hydrogel showing the cohesiveness in rheological measurement (left), and adhesiveness of the hydrogel on the skin (right).

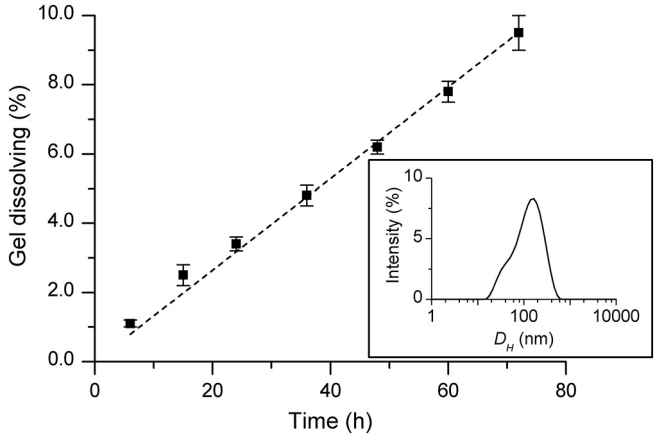

Fig. 11. Dissolving plot of the Calix-Cur hydrogel (37 °C) by concentration measurements of Cur in the supernatant. In the inset, the intensity (I)-weighted distribution of the hydrodynamic particle diameter of the Calix-Cur micellar nanoaggregates present in the release medium during the hydrogel dissolution.

4. Conclusions

In summary, a new biofriendly supramolecular nanohydrogel formed by a micellar polycationic choline-calix[4]arene derivative in the presence of curcumin was easily prepared in PBS medium at physiological pH, without additives and organic solvents, under stimulus concentration. The micellar nanohydrogel effectively solubilized curcumin, preserved the drug from chemical and photo-degradation and slowly dissolved releasing curcumin-loaded micelles with known drug delivery properties. The nanohydrogel matching the mechanical properties of self-healing and injectability with the benefits of a micellar nanocarrier exposing targeting ligands, appears a new promising soft material for drug delivery. Since curcumin is a multitarget drug, known as anti-inflammatory, antioxidant, antitumor, wound repairer, blue light filter, and agent for photodynamic therapy, the hydrogel is a potential candidate for multiple pharmaceutical applications. Noteworthy, we observed that other drugs can induce the gelation of the micellar choline-calixarene derivative, which appears to be a valid and versatile building block for the development of other functional nanohydrogels.

CRediT authorship contribution statement

Giuseppe Granata: Conceptualization, Formal analysis, Investigation, Methodology, Visualization. **Salvatore Petralia:** Conceptualization, Formal analysis, Investigation, Methodology, Writing - original draft, Writing - review & editing. **Giuseppe Forte:** Formal analysis. **Sabrina Conoci:** Investigation, Methodology. **Grazia Maria Letizia Consoli:** Conceptualization, Investigation, Supervision, Writing - original draft, Writing - review & editing.

Declaration of competing interest

The authors declare that they have no known competing financial interests or personal relationships that could have appeared to influence the work reported in this paper.

Acknowledgements

We thank Prof. S. Sortino (University of Catania) for his critical reading of the manuscript.

Appendix A. Supplementary data

AFM image of Calix-Cur hydrogel (Fig. S1); HOMO-LUMO structures for Cur and Calix-Cur (Fig. S2); absorption spectral changes of the hydrogel (Fig. S3) and Cur (Fig. S4) upon light exposure; forward and backward rheograms of the hydrogel at 25 and 37°C (Fig. S5); alternate step strain sweep test of the hydrogel (Fig. S6); creep-recovery behaviour of the hydrogel (Fig. S7); absorption spectra of the hydrogel at 25 and 75°C (Fig. S8); photographs of the hydrogel by heating (Fig. S9). Supplementary data to this article can be found online at https://doi.org/10.1016/j.msec.2020.110842.

References

[1] M. Mahinroosta, Z. Farsangi, Z. Shakoori, Hdrogels as intelligent materials: a brief review of synthesis, properties and application, Mater. Today Chem. 8 (2018) 42–55.
[2] E. Caló, V.V. Khutoryanskiy, Biomedical applications of hydrogels: a review of patents and commercial products, Eur. Polym. J. 65 (2015) 252–267.
[3] R. Narayanaswamy, V.P. Torchilin, Hydrogels and their applications in targeted drug delivery, Molecules 24 (3) (2019) 603.
[4] R. Dong, Y. Pang, Y. Su, X. Zhu, Supramolecula hydrogels: synthesis, properties and their biomedical applications, Biomater. Sci. 3 (2015) 937–954.
[5] M.H. Chen, J.J. Chung, J.E. Mealy, S. Zaman, E.C. Li, M.F. Arisi, P. Atluri, J.A. Burdick, Supramolecular hydrogel for biomedical applications, Macromol. Biosci. 19 (2019) 1800248.
[6] E. Ye, P.L. Chee, A. Prasad, X. Fang, C. Owh, V.J.J. Yeo, X.J. Loh, Supramolecular soft biomaterials for biomedical applications, Mater. Today 17 (4) (2014) 194–202.
[7] C. Dalwadi, G. Patel, Application of nanohydrogels in drug delivery systems: recent patents review, Recent pat. Nanotechnol. 9 (1) (2015) 17–25.
[8] W. Gao, Y. Zhang, Q. Zhang, L. Zhang, Nanoparticle-hydrogel: a hybrid biomaterial system for localized drug delivery, Ann. Biomed. Eng. 44 (6) (2016) 2049–2061.
[9] Z. Yinghao, Y. Xinru, C. Long, H. Jun, W. Liying, W. Jun, G. Shuyu, L. Wang, X. You, Q. Lou, S. He, J. Zhang, C. Dai, M. Zhao, M. Zhao, H. Hu, J. Wu, Biotherapeutic nanoparticles of poly(ferulic acid) delivering doxorubicin for cancer therapy, J. Biomed. Nanotechnol. 10 (2019) 1734–1743Cysteine-based redox-responsive nanoparticles for small-molecule agent delivery, Biomater. Sci. 7 (2019) 4218–4229.
[10] A.K. Mahanta, S. Senapati, P. Paliwal, S. Krishnamurthy, S. Hemalatha, P. Maiti, Nanoparticle-induced controlled drug delivery using chitosan-based hydrogel and scaffold: application to bone regeneration, Mol. Pharm. 16 (2019) 327–338.
[11] A. Altunbas, S.J. Lee, S.A. Rajasekaran, J.P. Schneider, D.J. Pochan, Encapsulation of curcumin in self-assembling peptide hydrogels as injectable drug delivery vehicles, Biomaterials 32 (2011) 5906–5914.
[12] For comprehensive reviews on calixarenes see: C.D. Gutsche, Calixarenes Revisited, Royal Society of Chemistry, Cambridge, 1998, Z. Asfari, V. Böhmer, J. Harrowfield, J. Vicens, Calixarenes 2001, Kluwer, Dordrecht, 2001.
[13] P. Neri, J.L. Sessler, M.-X. Wang, Calixarenes and beyond, Springer Verlag, 2016.
[14] R.V. Rodik, V.I. Boyko, V.I. Kalchenko, Calixarenes in biomedical researches, Curr. Med. Chem. 16 (13) (2009) 1630–1655.
[15] E.S. Español, M.M. Villamil, Calixarenes: generalities and their role in improving the solubility, biocompatibility, stability, bioavailability, detection, and transport of biomolecules, Biomolecules 9 (3) (2019) 90.
[16] S. Viola, G.M.L. Consoli, S. Merlo, M.A. Sortino, C. Geraci, Inhibition of rat glioma cell migration and proliferation by a calix[8]arene scaffold exposing multiple GlcNAc and ureido functionalities, J. Neurochem. 107 (2008) 1047–1055.
[17] G.M.L. Consoli, G. Granata, G. Fragassi, M. Grossi, M. Sallese, C. Geraci, Design and synthesis of a multivalent fluorescent folate–calix[4]arene conjugate: cancer cell penetration and intracellular localization, Org. Biomol. Chem. 13 (2015)

3298–3307.
[18] Y. Zhou, H. Li, Y.-W. Yang, Controlled drug delivery systems based on calixarenes, Chinese Chem. Lett. 26 (2015) 825–828.
[19] Z. Qi, C.A. Schalley, Exploring macrocycles in functional supramolecular gels: from stimuli responsiveness to systems chemistry, Acc. Chem. Res. 47 (2014) 2222–2233.
[20] T. Becker, C.Y. Goh, F. Jones, M.J. McIldowie, M. Mocerino, M.I. Ogden, Proline-functionalised calix[4]arene: an anion-triggered hydrogelator, Chem. Commun. (2008) 3900–3902.
[21] C.Y. Goh, T. Becker, D.H. Brown, B.W. Skelton, F. Jones, M. Mocerino, M.I. Ogden, Self-inclusion of proline-functionalised calix[4]arene leads to hydrogelation, Chem. Commun. 47 (2011) 6057–6059.
[22] Q. Zhao, Y. Chen, S.-H. Liab, Y. Liu, Tunable white-light emission by supramolecular self-sorting in highly swollen hydrogels, Chem. Commun. 54 (2018) 200–203.
[23] D. Hwang, J. Zhang, D.-S. Guo, L.-H. Wang, Z. Wang, Y. Liu, Supramolecular binary hydrogels from calixarenes and amino acids and their entrapment–release of model dye molecules, Soft Matter 7 (2011) 1756–1762.
[24] K.-P. Wang, Y. Chen, Y. Liu, A polycation-induced secondary assembly of amphiphilic calixarene and its multi-stimuli responsive gelation behavior, Chem. Commun. 51 (2015) 1647–1649.
[25] I. Di Bari, R. Picciotto, G. Granata, A.R. Blanco, G.M.L. Consoli, S. Sortino, A bactericidal calix[4]arene-based nanoconstruct with amplified NO photorelease, Org. Biomol. Chem. 14 (2016) 8047–8052.
[26] S. Hewlings, D.S. Kalman, Curcumin: a review of Its' effects on human health, Foods 6 (10) (2017) 92.
[27] G. Granata, I. Paterniti, C. Geraci, F. Cunsolo, E. Esposito, M. Cordaro, A.R. Blanco, S. Cuzzocrea, G.M.L. Consoli, Potential eye drop based on a calix[4]arene nanoassembly for curcumin delivery: enhanced drug solubility, stability, and anti-inflammatory effect, Mol. Pharm. 14 (2017) 1610–1622.
[28] R. Blanco, M. L. Bondì, G. Cavallaro, G. M. L. Consoli, E. F. Craparo, G. Giammona, M. Licciardi, G. Pitarresi, G. Granata, et al. Patent WO/2016/055976.
[29] R.V. Rodik, A.-S. Anthony, V.I. Kalchenko, Y. Mély, A.S. Klymchenko, Cationic amphiphilic calixarenes to compact DNA into small nanoparticles for gene delivery, New J. Chem. 9 (2015) 1654–1664.
[30] J. Li, Y. Guo, Y. Kuang, S. An, H. Ma, C. Jiang, Choline transporter-targeting and co-delivery system for glioma therapy, Biomaterials 34 (2013) 9142–9148.
[31] T. Yanai, D.P. Tew, N.C. Handy, A new hybrid exchange-correlation functional using the coulomb-attenuating method (CAM-B3LYP), Chem. Phy. Lett. 393 (2004) 51–57.
[32] J.P. Perdew, K. Burke, M. Ernzerhof, Generalized gradient approximation made simple, Phys. Rev. Lett. 77 (1996) 3865–3868.
[33] M. Cossi, N. Rega, G. Scalmani, V. Barone, Energies, structures, and electronic properties of molecules in solution with the C-PCM solvation model, J. Comput. Chem. 24 (2003) 669–681.
[34] A. Klamt, G. Schuurmann, COSMO: a new approach to dielectric screening in solvents with explicit expressions for the screening energy and its gradient, J. Chem. Soc. Perkin Trans. 2 (1993) 799–805.
[35] G.A. Di Labio, E.R. Johnson, A.O. de la Roza, Performance of conventional and dispersion-corrected density-functional theory methods for hydrogen bonding interaction energies, Phys. Chem. Chem. Phys. 15 (2013) 12821–12828.
[36] M.J.G. Peach, T. Helgaker, P. Sasek, T.W. Keal, O.B. Lutnaes, N.C. Handy, Phys. Chem. Chem. Phys. 8 (2006) 558–562.
[37] G. Consiglio, S. Failla, C.G. Fortuna, L. D'Urso, G. Forte, Aggregation of a Zn(II)-salen complex: theoretical study of structure and spectra, Comp. Theor. Chem. 1067 (2015) 1–6.
[38] R.E. Stratmann, G.E. Scuseria, M.J. Frisch, An efficient implementation of time-dependent density-functional theory for the calculation of excitation energies of large molecules, Chem. Phys. 109 (1998) 8218–8224.
[39] G. Scalmani, M.J. Frisch, B. Mennucci, J. Tomasi, R. Cammi, V. Barone, Geometries and properties of excited states in the gas phase and in solution: theory and application of a time-dependent density functional theory polarizable continuum model, J. Chem. Phys. 124 (2006) 094107.
[40] R. Benassi, E. Ferrari, S. Lazzari, F. Spagnolo, M. Saladini, Theoretical study on curcumin: a comparison of calculated spectroscopic properties with NMR, UV–vis and IR experimental data, J. Mol. Struct. 892 (2008) 168–176.
[41] E. Ferrari, M. Asti, R. Benassi, M. Saladini, Metal binding ability of curcumin derivatives: a theoretical vs. experimental approach, Dalton Trans. (15) (2013) 5304–5313.
[42] X.Z. Zhao, T. Jiang, L. Wang, H. Yang, S. Zhang, P. Zhou, Interaction of curcumin with Zn(II) and cu(II) ions based on experiment and theoretical calculation, J. Mol. Struct. 984 (2010) 316–325.
[43] R. Benassi, E. Ferrari, S. Lazzari, F. Pignedoli, F. Spagnolo, M. Saladini, How glucosylation triggers physical–chemical properties of curcumin: an experimental and theoretical study, J. Phys. Org. Chem. 24 (2011) 299–310.
[44] A.V. Marenich, C.J. Cramer, D.G. Truhlar, Universal solvation model based on solute electron density and on a continuum model of the solvent defined by the bulk dielectric constant and atomic surface tensions, J. Phys. Chem. 113 (2009) 6378–6396.
[45] I. Di Bari, A. Fraix, R. Picciotto, A.R. Blanco, S. Petralia, S. Conoci, G. Granata, G.M.L. Consoli, S. Sortino, Supramolecular activation of the photodynamic properties of porphyrinoid photosensitizers by calix[4]arene nanoassemblies, RSC Adv. 6 (2016) 105573–105577.
[46] I. Di Bari, G. Granata, G.M.L. Consoli, S. Sortino, Simultaneous supramolecular activation of NO photodonor/photosensitizer ensembles by a calix[4]arene nanoreactor, New J. Chem. 42 (2018) 18096–18101.
[47] M. Pekař, Hydrogels with micellar hydrophobic (nano)domains, Front. Mater. 1 (2015) 1–14.
[48] D. Yanagisawa, N. Shirai, T. Amatsubo, et al., Relationship between the tautomeric structures of curcumin derivatives and their Abeta-binding activities in the context of therapies for Alzheimer's disease, Biomaterials 31 (2010) 4179–4185.
[49] S. Ghosh, S. Mondal, Spectroscopic study on the interaction of medicinal pigment, curcumin with various surfactants: An overview, J. Surf. Sci. Technol. 28 (2012) 179–195.
[50] M.H.M. Leung, H. Colangelo, T.W. Kee, Encapsulation of curcumin in cationic micelles suppresses alkaline hydrolysis, Langmuir 24 (2008) 5672–5675.
[51] A.A. Reinke, J.E. Gestwicki, Structure-activity relationships of amyloid beta-aggregation inhibitors based on curcumin: influence of linker length and flexibility, Chem. Biol. Drug Des. 70 (2007) 206–215.
[52] U.C. Singh, P.A. Kollman, An approach to computing electrostatic charges for molecules, J. Comp. Chem. 5 (1984) 129–145.
[53] B.H. Besler, K.M. Merz Jr., P.A. Kollman, Atomic charges derived from semi-empirical methods, J. Comp. Chem. 11 (1990) 431–439.
[54] Y.J. Wang, M.H. Pan, A.L.I. Cheng, L. Lin, Y.S. Ho, C.Y. Hsieh, J.K. Lin, Stability of curcumin in buffer solutions and characterization of its degradation products, J. Pharm. Biomed. Anal. 15 (1997) 1867–1876.
[55] W. Ostwald, About the mathematical representation of the structural area of the viscosity, Kolloid Zeitschrift 47 (1929) 176–187.
[56] J. Qu, X. Zhao, P.X. Ma, B. Guo, pH-responsive self-healing injectable hydrogel based on N-carboxyethyl chitosan for hepatocellular carcinoma therapy, Acta Biomater. 58 (2017) 168–180.
[57] J. Qu, X. Zhao, Y. Liang, T. Zhang, P.X. Ma, B. Guo, Antibacterial adhesive injectable hydrogels with rapid self-healing, extensibility and compressibility as wound dressing for joints skin wound healing, Biomaterials 183 (2018) 185–199.
[58] Z. Deng, Y. Guo, X. Zhao, P.X. Ma, B. Guo, Multifunctional stimuli-responsive hydrogels with self-healing, high conductivity, and rapid recovery through host–guest interactions, Chem. Mater. 30 (2018) 1729–1742.
[59] A.P. Mathew, S. Uthaman, K.-H. Cho, C.-S. Cho, I.-K. Park, Injectable hydrogels for delivering biotherapeutic molecules, Int. J. Biol. Macromol. 110 (2018) 17–29.
[60] J. Hurler, A. Engesl, B.P. Kermany, N. Skalko-Basnet, Improved texture analysis for hydrogel characterization: gel cohesiveness, adhesiveness, and hardness, J. Appl. Polym. Sci. 125 (1) (2012) 180–188.
[61] A.M. Grillet, N.B. Wyatt, L.M. Gloe, Polymer gel rheology and adhesion, in: J. De Vicente (Ed.), Rheology, InTech, Rijeka, 2012, pp. 59–80 chapter 3.